VII. Applied Mechanics

ENGINEERING MECHANICS DIVISION

A. Simulation of Venus Atmospheric Entry by Earth Reentry,[1] *J. M. Spiegel, F. Wolf, and D. W. Zeh*

1. Introduction

Each time a new unmanned entry mission to Mars or Venus is considered, the question of the value of an earth reentry test invariably arises. That is, can it be shown that the simulation of entry dynamics, heating, and heat shield response is adequate? This question arises from the well-known fact that the atmospheric composition and effective scale heights of the inner planets differ from that of earth.

Although the atmospheric compositions of Mars and Venus are now considered to be similar (mostly carbon dioxide), the lower velocities for Mars entry place the environment of heat shield materials of test specimen size within the reach of ground-based test facilities, whereas similar tests for direct Venus entry are, at present, marginal at best (SPS 37-49, Vol. III, pp. 141–152). Since analytical methods are still somewhat uncertain for predicting mass loss rates at Venus entry conditions (SPS 37-49, Vol. III, pp. 141–152), even one flight qualification test for this subsystem alone would be significant if it can be shown that the earth environment is comparable in severity and sufficiently similar to Venus entry.

Past work on the subject of planetary entry simulation by earth reentry (Refs. 1, 2, and 3) has emphasized many aspects of the problem, but little attention has been directed toward identifying the specific differences in radiative heat transfer and heat shield response, both of which might be expected to be particularly sensitive to chemical differences in atmospheric composition. It is concluded by H. Kennet (Ref. 1) that simultaneous simulation of all entry environments in a single flight test is not feasible, but that selected simulation can be achieved (Refs. 1 and 3). However, no conclusions were obtained regarding the response of an ablating heat shield.

In the present study, it was accepted at the outset that complete simulation is unlikely, but it was also postulated that the lack of simulation might be of an acceptable magnitude for proof test purposes. Time histories of acceleration, angle-of-attack envelope, entry heating, and heat shield ablator response were calculated at two locations on a spherically-blunted, 60-deg half-angle conical body to determine the best match of path angles and the degree of simulation attainable for the four factors specified.

[1]This article is a condensation of a paper of the same title to be presented at the AIAA Entry Vehicle Systems and Technology Conference, Williamsburg, Va., December 3–5, 1968.

2. Methods of Approach

a. Entry conditions. The entry-body configuration and other related factors used in this study are shown on Fig. 1. This configuration was chosen as a representative case although there are various reasons why a larger nose radius or a smaller cone angle might be more desirable. The entry angle-of-attack was taken as 50 deg; the initial pitch, yaw, and roll rates were taken as zero. At station 0.8r, the shock stand-off distance and wave angle were obtained from available flow-field solutions.

All conditions specified on Fig. 1 were used throughout the study for both earth and Venus entries.

b. Trajectory and heating. Entry trajectories, dynamic motion, and heat transfer were calculated with a modified version of a computer program (designated 1880)

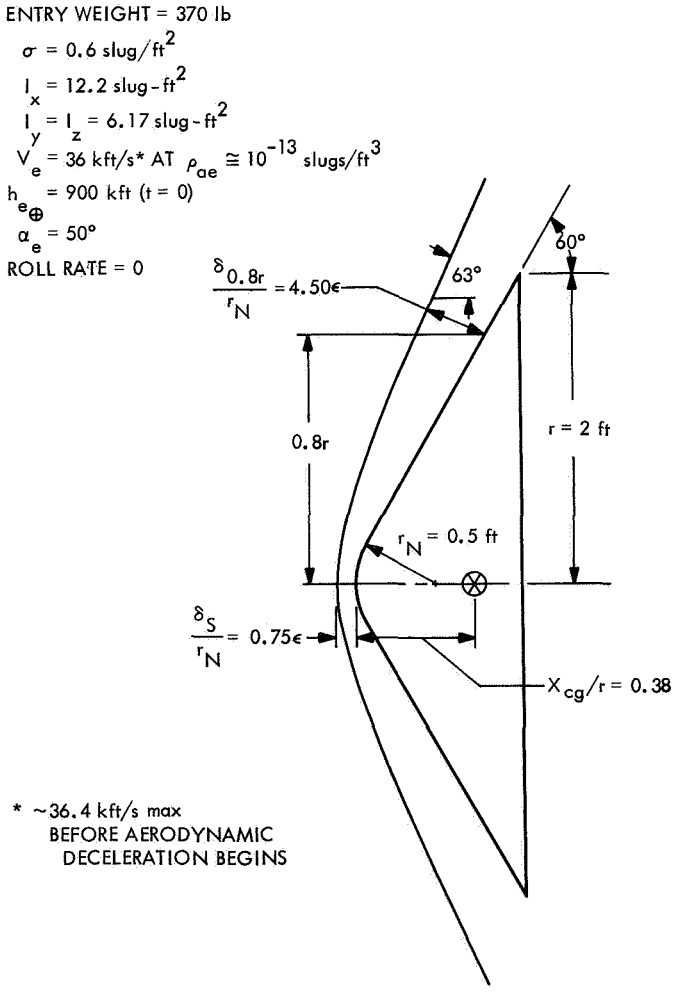

Fig. 1. Entry body configuration and flight conditions

originally developed by the AVCO Corporation for JPL and described in Refs. 4 and 5. Density and temperature profiles for earth and Venus were taken from Refs. 6 and 7, respectively. Reference 7 presents two basic model atmospheres (obtained from the *Mariner* Venus 67 and *Venera 4* probes) of which MV-3 was selected because the presence of N_2 in addition to CO_2 was expected to yield the highest radiative heat transfer. The mixture was approximated as 90% CO_2 and 10% N_2.

Stagnation point convective heat transfer was computed from a density, velocity, and molecular weight correlation originally built into the trajectory program and modified to agree with the results given in Refs. 8 and 9. Convective heating at a 0.8r station location on the conical region of the entry body was taken as 0.30 of the stagnation value based on available published and unpublished information. For local Reynolds numbers above 300,000, based on wetted distance from the stagnation point to the body edge, turbulent heating was assumed at the 0.8r station location, as computed by an appropriate expression built into program 1880.

Radiative heating was computed for both the stagnation point and a point on the cone (0.8r) (Fig. 1) using the slab approximation. Molecular bands, atomic lines, and continuum radiation sources are included. The air calculations were obtained by combining shock layer data from the trajectory program 1880 with radiation data from Ref. 10. The nonair calculations were obtained from program 1880 by a newly added routine based on the Kivel–Bailey method (Ref. 11) above a wavelength of 2000 Å, supplemented by vacuum ultra-violet contributions of C, N, and O lines as well as the CO(4+) band systems. Gaseous self-absorption is accounted for in an approximate manner, but radiation cooling and ablation product radiation interactions are not included. For comparative purposes, and for the velocity ranges considered, this omission is judged to be acceptable. The nonequilibrium contribution was treated in the manner described in Ref. 12 as incorporated in program 1880.

c. Heat shield response. The in-depth response of a charring ablator heat shield for the earth and Venus entries considered herein was calculated using the Equilibrium Surface Thermochemistry (EST) (Ref. 13) and Charring Material Ablation (CMA) (Refs. 14 and 15) computer programs developed by the Aerotherm Corporation for the NASA Manned Spacecraft Center. The CMA program gives a realistic description of chemical interaction between ambient and heat shield species and, therefore, met the requirements of the present study.

These requirements were to determine the effects of differing ambient gas composition on heat shield response during an earth flight simulation of Venus entry.

The heat shield was assumed to be made of high-density phenolic nylon (75 lb/ft^3, 50% phenolic resin and 50% nylon resin by weight) of sufficient thickness to approximate a semi-infinite body. Although materials forming stronger chars may be preferable for the actual heat shield, phenolic nylon was chosen both because it adequately characterizes the chemical response of many other charring ablators and because of the availability of input data necessary for the CMA program. Thermophysical properties were taken from Ref. 16; kinetic data was taken from Ref. 17.

Assumptions and uncertainties in the analysis that may affect final heat shield design, but are not likely to affect the qualitative results of the present study, include the following:

(1) All diffusion coefficients are assumed equal in the boundary layer.

(2) The heat transfer coefficient and mass transfer coefficient are assumed equal.

(3) Substantial uncertainties exist for kinetic and thermophysical data for the heat shield material.

(4) Internal reactions between pyrolysis gases and char have been ignored, as has char shrinkage.

(5) Mechanical char removal has been ignored; this could be most important, as noted later.

(6) Equilibrium conditions exist at the heat shield surface between the char, pyrolysis gases, and ambient species.

3. Results and Discussion

a. Entry path angle for simulation. An examination of approximate scaling rules and atmospheric density profiles for earth and Venus in the region of maximum heating and deceleration led to the preliminary finding that 45 deg is the steepest Venus entry that could be simulated by earth reentry. The final selection of an entry angle (γ_e) for a Venus trajectory that would be best simulated by a vertical earth entry was made by fixing all entry conditions as shown in Fig. 1 while varying γ_e and investigating the resulting simulation of deceleration and heating rates, integrated heating, and heat shield mass loss. On this basis, a 40-deg Venus entry was selected, and all subsequent discussion will relate to the simulation of this case by a vertical earth entry.

b. Trajectory and heat transfer simulation. Time histories of deceleration and angle-of-attack envelope were calculated to be quite similar for the 40-deg Venus and vertical earth entries, except that maximum deceleration is predicted to be about 18% higher for earth entry.

Time histories of convective heat transfer are presented in Figs. 2(a1) and 2(a2). The simulation is observed to be good for both the stagnation point and the 0.8r case. Transition to turbulent flow at 0.8r is predicted to occur at about the time of maximum stagnation point heating.

Time histories of radiative heat transfer are presented in Figs. 2(b1) and 2(b2). The stagnation point heating pulses appear quite similar in both atmospheres, except for the relatively later onset of the equilibrium radiation during Venus entry. The stagnation point maximum radiative transfer for air occurs at a velocity of 34,000 ft/s and at a shock layer temperature (T_{SL}) $\cong$ 11,000°K where the radiation is primarily atomic in nature. At the corresponding point in the Venus entry trajectory, the temperature is more than 1000°K lower, thereby depressing atomic sources, but still above the level at which substantial quantities of CO molecules are formed. The peak Venus radiation comes primarily from the CO(4+) molecular band system at wavelengths < 0.2 μ, and occurs at a velocity of 30,000 ft/s where $T_{SL} \cong 8400$°K. Therefore, the delay in the occurrence of peak radiative transfer for Venus relative to earth entry is attributable to the differences in chemical composition of the respective atmospheres.

At the 0.8r station of the entry body, the radiative heat pulses for Venus and earth are quite different in shape and magnitude as seen in Fig. 2(b2). There, shock layer temperatures at maximum radiative heating ($V \cong 30{,}000$ ft/s) are around 7700°K for both entry cases. At this temperature, air has no radiating species comparable in intensity to CO and CN. This explains the large peak for Venus entry, compared to the almost constant air radiation, and the large difference in the maximum radiative rates. This breakdown of similarity of radiative transfer distribution around the body, as for the stagnation point, also stems from the chemical difference of the two atmospheres and probably is not adjustable either by modification of entry conditions or any other factors.

c. Heat shield response simulation. Comparison of heat shield response for the 90-deg earth entry and 40-deg Venus entry is provided in Figs. 2(c1), 2(c2), 2(d1), and 2(d2) for both the stagnation point and the 0.8r location.

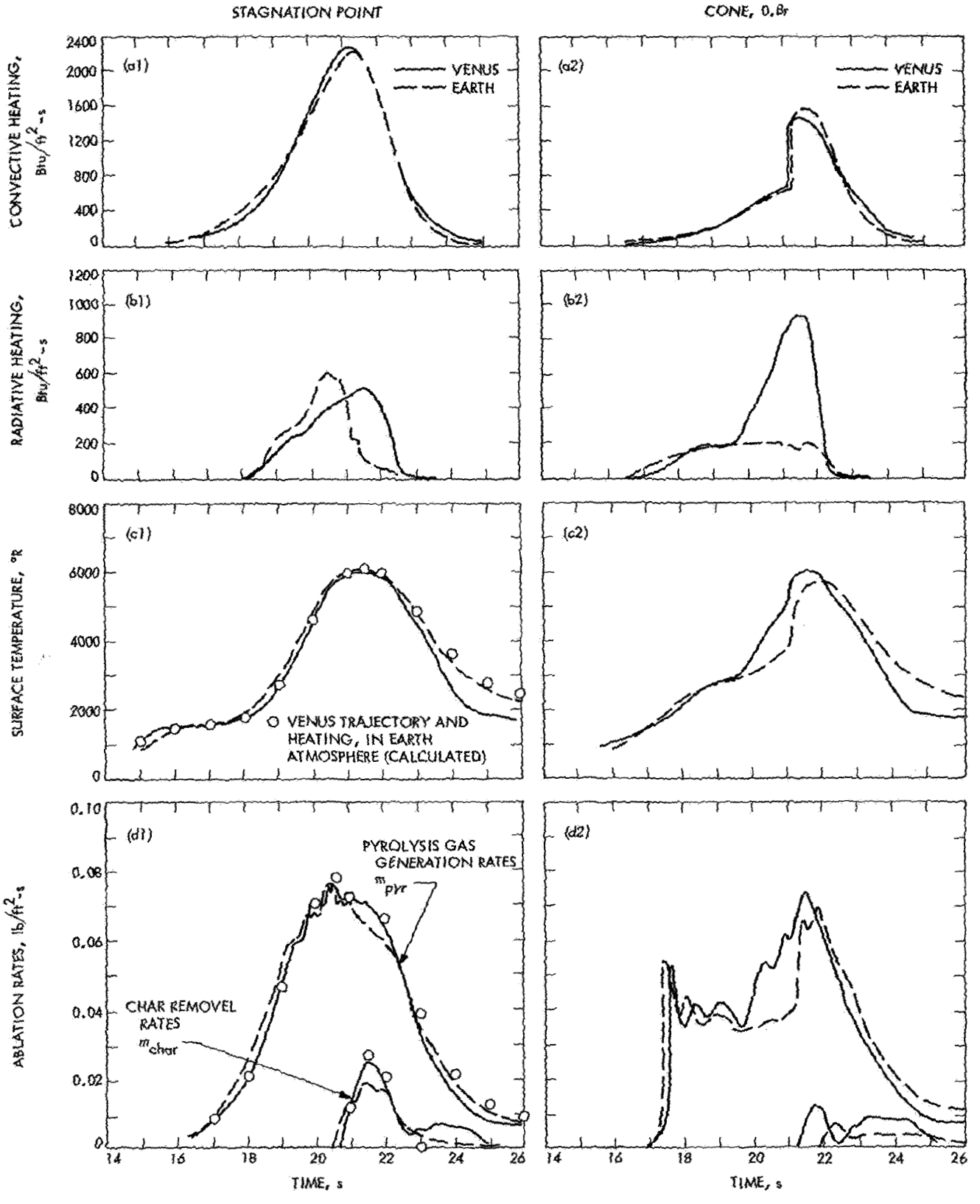

Fig. 2. Comparison of earth and Venus entry

Although the applied heating pulses are quite smooth, the curves representing ablation rates are irregular. Such irregularities or oscillations are inherent in the computational procedure and are not representative of any real physical process; they are discussed in some detail in Ref. 14 and shown to be characteristic only of materials, such as nylon, that decompose rapidly. Most important, it was found that the oscillations had relatively little effect on overall ablation response. In the present case, the oscillations in the predicted pyrolysis gas generation rates appear to be sufficiently small that even the detailed nature of ablation response is relatively unmasked.

Time histories of applied heating, surface temperature and ablation rates, have been vertically aligned in Fig. 2 to simplify visualization of ablation response. The first obvious conclusion upon inspection of these figures is that, within the limitations of the present analysis, simulation of the heat shield response for the 40-deg Venus entry by the 90-deg earth entry is remarkably good during the entire heating pulse at both the stagnation point and the 0.8r location. This, in the face of somewhat different radiative heating pulses, particularly at the 0.8r location, is indicative of the flexible, self-regulating, "heat-absorption" mechanisms of a charring ablator.

The most important of these mechanisms are convective blockage by ablation gases, reradiation at high surface temperatures, and endothermic char removal (sublimation and reaction with hydrogen in pyrolysis gases). It is important to note that the latter two mechanisms are critically dependent upon the presence of the char and are largely responsible for the comparable ablation response for the Venus and earth entries in spite of somewhat different applied heating rates. If the char were lost by thermomechanical means, pyrolysis rates would increase markedly and would be much more sensitive to applied heating rates.

It is apparent from the close agreement in ablation response for the Venus and earth entries that direct chemical effects due to ambient gas composition are negligible. To demonstrate this even more clearly, the CMA program was run using the 40-deg Venus entry conditions but assuming an air atmosphere. These results, shown as circles in Figs. 2(c1) and 2(d1), follow the true Venus calculations very closely up to about 22 s, and indicate that the assumed ambient gas composition is unimportant. After this time, the ambient gas effects become noticeable and the calculations follow the earth results, as would be expected since an air atmosphere was assumed. The surface temperatures and pyrolysis rates are somewhat higher for the earth entry in this region since the chemical reactions between ambient species and ablation products are relatively more exothermic in air than in the assumed Venus atmosphere. In any case, these chemical effects are clearly not important in determining overall heat shield response.

It should be emphasized that the above remarks on heat shield response are valid only within the framework of the ablation model used. It is equally important to note, however, that an actual flight test is, at present, the only means of determining whether other ablation mechanisms may be active and/or controlling during Venus entry since the entry conditions cannot be simulated fully with existing ground facilities. It has been shown that the heating, pressure, and, hence, shear histories of a 40-deg Venus entry can be closely simulated by a 90-deg earth entry, and that the ambient gas composition has negligible direct effect on ablation response. Hence, any unidentified ablation mechanisms such as thermomechanical char removal that might occur in the Venus entry should also appear in the earth flight test.

d. Launch vehicle considerations. The need for a near-vertical earth atmospheric entry at about 36,000 ft/s to simulate a Venus entry at path angles up to 40 or 50 deg for about a 4-ft diameter, 400-lb vehicle places stringent requirements on the launch system. Existing applicable systems are both costly ($2–$4 $\times$ 10^6) and, in their current state, flight tested to operate only at shallow (0–15 deg) entry path angles.

One means of alleviating the size and weight requirement, with a possibly acceptable compromise in simulation, is to essentially truncate a full-scale entry configuration at a location that permits full-scale simulation of the stagnation region. Under these conditions, the best choice at this time for a launch vehicle of modest cost would appear to be the (prospective) Athena Super H, of which the three upper stages are in existence and have been flown.

4. Conclusions

For the Venus entry mission considered herein, a full-scale vertical earth reentry flight test at the same ballistic coefficient and entry velocity should provide an acceptable simulation of deceleration, dynamic motion, and heat shield response at a Venus path angle of about 45 deg despite significant differences in radiative heating.

Since a full-scale test imposes stringent requirements on the launch system for such a test, a compromise test

configuration is possible in which a full-scale configuration is truncated at a location that permits full-scale simulation of the nose region only.

When some compromises are accepted, it appears that a meaningful earth reentry test of a simulated full-scale aeroshell (or part thereof) for the Venus case considered herein could be made. As a minimum, the earth reentry test can place a Venus capsule in a flight environment comparable in severity to actual Venus entry. This environment is difficult to obtain in ground facilities for any significant piece of flight hardware.

References

1. Kennet, H. and Taylor, R. A. "Earth Reentry Simulation of Planetary Entry Environment," *J. Spacecraft Rockets,* Vol. 3, pp. 504–512, 1966.
2. Beuf, F. G., Katz, G. D. and Kern, R. J., "Earth Entry Flight Test of Mars Entry Vehicles," *J. Spacecraft Rockets,* Vol. 3, pp. 498–503, 1966.
3. Stimpson, L. D., "Earth Simulation of Planetary Entry," Paper 65-442, presented at the AIAA Second Annual Meeting, San Francisco, Calif., July 26–29, 1965.
4. *Mars-Venus Capsule Parameter Study,* Technical Report 64-1, Vols. I, II, III. AVCO Corporation, Research and Advanced Development Division, Wilmington, Mass., Jan.–Mar. 1964.
5. *JPL Entry Vehicle Design Computer Program Users Manual,* Scientific and Technical Aerospace Report N67-13141. AVCO Corporation, Space Systems Division, Lowell, Mass., Dec. 1, 1966.
6. *U.S. Standard Atmosphere, 1962,* U.S. Government Printing Office, Washington, Dec. 1962.
7. Schiffer, R. A., "Engineering Models of the Venus Atmosphere Based on an Interpretation of Recent Space Observations of Venus," submitted for presentation at AIAA Seventh Aerospace Sciences Meeting, New York, Jan. 20–22, 1969.
8. Hoshizaki, H., "Heat Transfer in Planetary Atmospheres at Super-Satellite Speeds," *ARS J.,* Vol. 32, pp. 1544–52, Oct. 1962.
9. Marvin, J. G., and Deiwert, G. S., *Convective Heat Transfer in Planetary Atmospheres,* NASA TR R-224. National Aeronautics and Space Administration, Washington, 1965.
10. Page, W. A., *et al.,* "Radiative Transport in Inviscid Non-Adiabatic Stagnation-Region Shock Layers," Paper 68-784, presented at the AIAA Third Thermophysics Conference, Los Angeles, Calif., June 1968.
11. Kivel, B., and Bailey, K., *Tables of Radiation from High Temperature Air,* AVCO–Everett Research Laboratory Research Report 21. AVCO Corporation, Everett, Mass., 1957.
12. Wolf, F., and Spiegel, J. M., "Status of Basic Shock-Layer Radiation Information for Inner-Planet Atmospheric Entry, *J. Spacecraft Rockets,* Vol. 4, pp. 1166–1173, 1967.
13. *Aerotherm Equilibrium Surface Thermochemistry Program, Version 2, User's Manual,* Aerotherm Corporation, Palo Alto, Calif., June 1966.
14. Moyer, C. B., and Rindal, R. A., *An Analysis of the Coupled Chemically Reacting Boundary-Layer and Charring Ablator: Part II, Finite Difference Solution for the In-Depth Response of Charring Materials Considering Surface Chemical and Energy Balances,* Final Report 66-7. Prepared for the NASA Manned Spacecraft Center under contract NAS 9-4599. Aerotherm Corporation, Palo Alto, Calif., Mar. 14, 1967. Also available as NASA CR-1061, National Aeronautics and Space Administration, Washington, June 1968.
15. *Aerotherm Charring Material Ablation Program, Version 2, User's Manual,* Aerotherm Corp., Palo Alto, Calif., Jan. 1966.
16. Wilson, R. G., *Thermophysical Properties of Six Charring Ablators from 140 to 700°K and Two Chars from 800 to 3000°K,* NASA TN D-2991, National Aeronautics and Space Administration, Washington, Oct. 1965.
17. Rindal, R. A., and Kratsch, K. M., *Prediction of the Ablative Material Performance on a Scout Entry Vehicle,* Final Report 66-4. Prepared for the NASA Ames Research Center under contract NAS 2-3587. Aerotherm Corporation, Palo Alto, Calif., July 1966.

B. Mobility and Wheel–Soil Interaction: Study and Tests, *I. Kloc*

1. Introduction

This article presents an outline of the basic theoretical concepts and analysis being used to determine the bearing capacity and the pressure–sinkage relationships of soft soil surfaces when subjected to uniform vertical or inclined loads. This study is being implemented by an exploratory testing program. The results of both analysis and tests will be used to evaluate mobility performance of planetary roving vehicles.

The need for this analysis arises due to the practical impossibility of obtaining bearing capacity values and pressure–sinkage relationships by direct tests as done on earth over potentially known and accessible environments. Faced with this problem, the objectives of this study are as follows:

(1) Theoretical determination of the ultimate pressure load of horizontal or sloping lunar surfaces.

(2) Determination of soft soil surface pressure–sinkage relationships to evaluate lunar vehicle performance on horizontal and sloping surfaces.

(3) Testing to see if the pressure–sinkage relationships can be predicted by using the ultimate pressure load formulation as a function of depth below the surface.

This study relates mainly to the safety and performance of vehicles operating over horizontal soil surfaces or when climbing, descending, or traversing a sloping ground. For testing purposes, and to verify the theory, use is made of a cohesionless soil (sand).

2. Soil Bearing Capacity Problem

Currently, there is no general and reliable theoretical formulation, based upon tests, that presents the influence of terrain slope on the soil bearing capacity. Available solutions provide only the ultimate bearing load applied uniformly on an infinitely long strip over a horizontal terrain. A solution of this problem, applying the method of characteristics, was obtained by V. V. Sokolovsky (Ref. 1) who also considered inclined loads. An approximate solution to the same problem was obtained by K. Terzaghi (Ref. 2) and improved by G. G. Mayerhof (Ref. 3) who expanded the results (Ref. 4) to include oblique loads over horizontal terrains. This author also studied the case of vertical loads applied on slopes (Ref. 5) considering either purely cohesive or cohesionless soils only, a limitation which restricts its general and practical application. Recently, L. L. Karafiath (Ref. 6), following Terzaghi's basic concepts, formulated the ultimate (vertical or oblique) load on the slopes. No load optimization or tests were made to better define and verify the results. Since the problem at hand is of non-linear character and the methods of approximation resort to the principle of linear superposition, it is impossible to state the degree of approximation obtained.

As an attempt to solve the problem of ultimate load on sloping surfaces, it is considered that the application of limit load analysis of the theory of plasticity to soil mechanics will permit a satisfactory solution. In this context, the theorems of collapse load of limit analysis define upper and lower bound loads between which lies the ultimate load. A proper selection of both velocity and stress field pattern permits narrowing the interval of these bounds, and a better definition of the ultimate load is obtained. The identity of both the upper and lower bounds is a sufficient condition to define the true maximum load.

Plastic limit analysis theory was used in the study of the vertical punch indentation problem of soils by R. T. Shield (Ref. 7). A rather large difference between bounds was obtained for friction angles between 30 and 40 deg, of particular interest to lunar soils. Furthermore, the soil was considered weightless although this factor bears significantly on the ultimate load value. To obviate these limitations, the present analysis considers the soil weight and attempts to narrow the interval between the limiting loads.

To this effect, a theoretical study was done and numerical results have been obtained that define the upper limit load of the lunar surface when subjected to a quasi-static vertical or inclined load applied on an infinitely long strip of known width resting either on a horizontal surface or along a sloping terrain (Fig. 3). The solution accounts for the influence of footing depth, soil weight, friction, and cohesion. The load is minimized by optimizing the failure angle ψ.

It is assumed that the lunar soil behaves as a rigid plastic material that follows the Coulomb–Mohr failure condition for soils and its associated flow rule. This criterion satisfies reasonably well the expected failure modes and the character of the lunar soil as described by its mechanical properties, which are approximately as follows: the angle of internal friction, 37 ± 2 deg; cohesion, 0.06 psi; and unit weight in the lunar gravitational field, 15 ± 2 lb/ft^2. A computer program was developed that accounts for all these factors. The general form of the ultimate pressure load[2] is

$$p = c(N_c)_{\alpha,\delta} + \gamma z(N_q)_{\alpha,\delta} + \tfrac{1}{2}\bar{B}\gamma(N\gamma)_{\alpha,\delta}$$

where

p = ultimate pressure

c = soil cohesion

z = depth below surface

$\bar{B}$ = pad width

N_c, N_q, N_δ = bearing capacity coefficients functions of ϕ, α, and δ

ϕ = soil friction

α = terrain slope

δ = load inclination with reference to local vertical

γ = soil unit weight

This study, now in process, attempts to define the lower bound load that results from an appropriate selection of a stress field pattern. It is futher emphasized that the infinite strip direction is horizontal across the slope and

[2]Kloc, I., *Load Bearing Capacity Bounds of Sloping Soil Surfaces* (to be published).

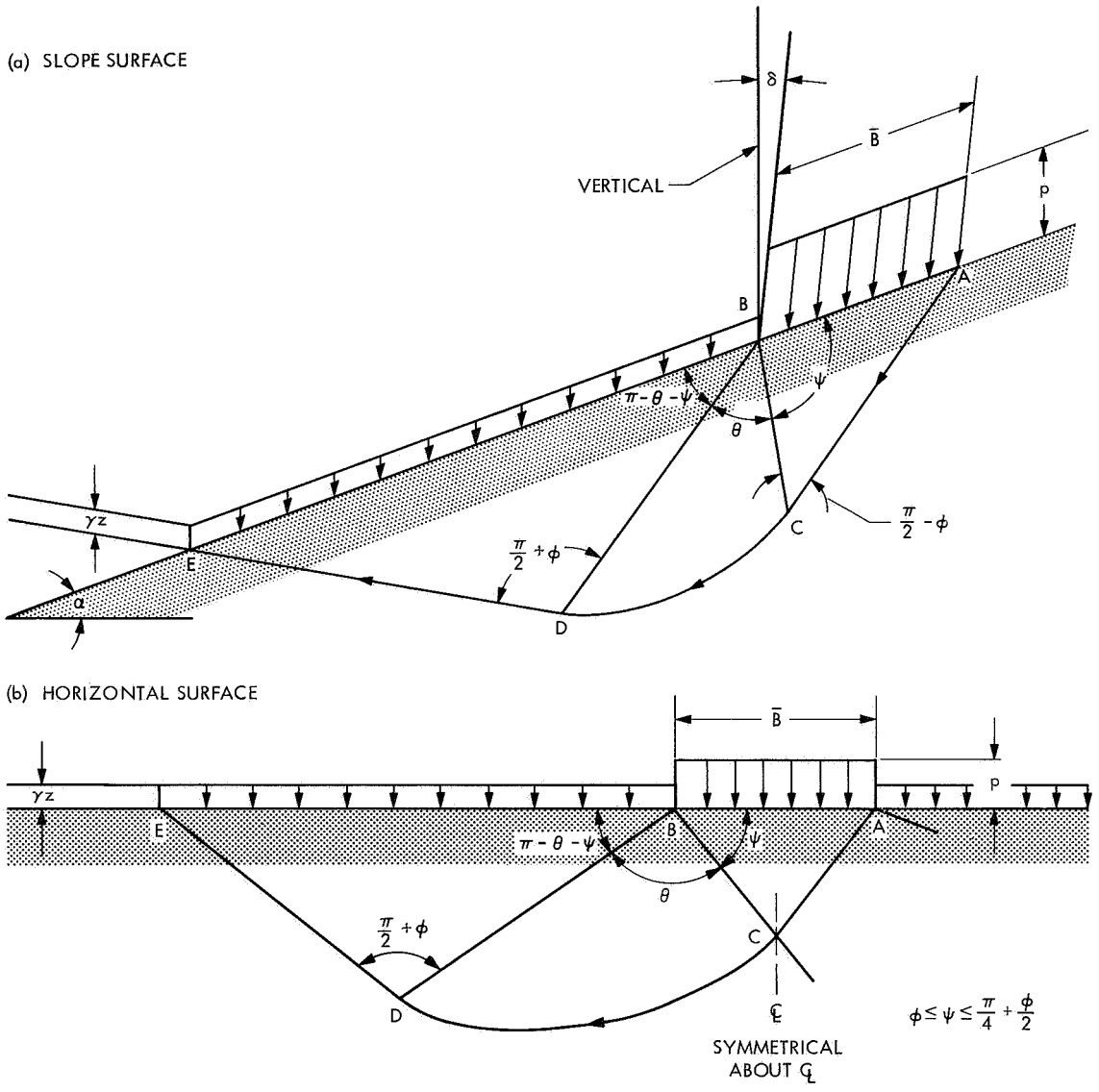

Fig. 3. Soil failure mechanisms

not up, down, or at the top of the slope (rim of a lunar crater). Each of these cases requires a separate study which can be done based on the same method of solution.

In the application of the numerical data, extreme care should be exercised when trying to extend the results of an infinite strip to a finite circular, rectangular, or elliptical load pattern. These factors should be interpreted in the light of the three-dimensional criteria of soil failure which, in the present state of theoretical soil mechanics, are still under discussion and experimentation. Nevertheless, an attempt is being made to better define and improve on the currently available concepts.

3. Extension of Analysis

The importance of the various stability conditions to which the planetary roving vehicle will be subjected as it traverses sloped surfaces cannot be over-emphasized. The sorting out, and overriding of obstacles can always be managed on a go/no-go basis as long as the vehicle has the required power and discrimination capability to operate accordingly. When faced with the maximum support that the ground can provide, the soil mechanical properties and lunar topography, slopes, and regions of slope changes play an important role in disclosing the potential risks of the vehicle becoming immobilized. This eventuality may be caused either by excessive sink-

age or the existence of weakening tension cracks around the periphery of a crater edge. In the latter case, a state of failure could result in a pronounced tilting of the vehicle accompanied by a loss of stability. Within the same analytical framework, an extension of this study could cover the ultimate load a lunar crater edge can support.

4. Testing Program

The following exploratory testing program describes the basic information, methods, and procedures required to corroborate the load-bearing capacity values and the pressure–sinkage relationships to be used in connection with lunar surface vehicle mobility studies. Specific information is given with reference to equipment handling, instrumentation, soil preparation, and generation of testing data. The purpose of these tests is to disclose the soil failure character and response (load versus displacement) of the following two principal soil surface types:

(1) Horizontal soil surface.

(2) Sloping soil surface.

In both cases, the applied loads are uniform and vertical. In the case of horizontal surfaces, the displacements are restricted to develop along the vertical direction only. For sloping surfaces, the bearing plates are guided and displacements may occur simultaneously in the vertical and horizontal directions.

Plate–soil contact starts either on or at a specified depth below the surface. In all cases, during the penetration process, the bearing plates are maintained parallel to the original soil surface.

The objectives of the tests are as follows:

(1) To verify the analytical approach that formulates the bearing capacity of horizontal and sloping terrain surfaces subjected to quasi-static uniform vertical loads.

(2) To find out if the bearing capacity of cohesionless soil surface slopes can be predicted up to slopes equivalent to the soil angle-of-repose.

(3) To qualify the semiempirical procedure designed to estimate the pressure–sinkage relationships whereby a single continuous load penetration test may be approximated by a series of load bearing capacities as functions of the depth below the terrain surface.

(4) To compare the influences of plate size and geometry (rectangular, square, circular, and wheel shapes) on the soil bearing capacity and pressure–sinkage relations.

a. Test box and soil hopper. A plywood box reinforced with peripheral aluminum corner angles is provided to contain the soil material (Fig. 4). The inside box dimensions are $28 \times 38 \times 30$ in. deep. Box dimensions are established to minimize the wall boundary effects for the selected bearing plates. Special aluminum guides are provided to support a metal straight edge that smooths the soil surface to prescribed heights and slopes. An overhead crane picks up the box by means of four steel cables attached to the corners and carries it to the load testing machine.

A specially designed wood hopper ($26 \times 11.5 \times 13$ in. high) permits the soil to flow down into the test box at a controlled rate and height while it displaces horizontally and/or vertically (Fig. 4). The bottom of the hopper has an adjustable gap that permits control of the sand flow. The soil is deposited in the test box under similar conditions of flow rate and height. This generates an artificial sand bed of homogeneous and reproducible granular structure over a wide range of densities.

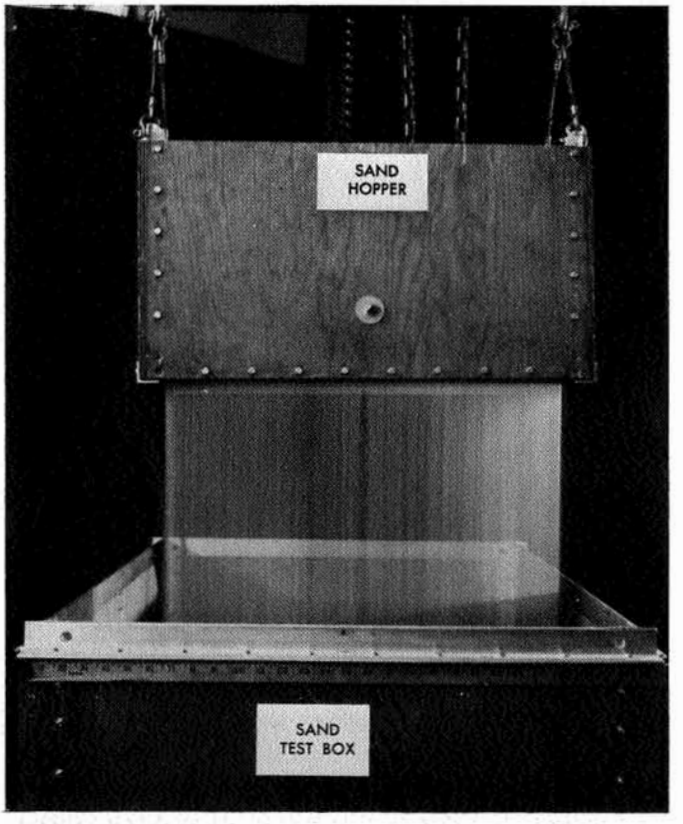

Fig. 4. Control of sand density

b. Soil material. The soil material selected is an air-dried, coarse, medium-to-fine white silica sand. Penetration tests are done on a compact sand in which a shear-type failure can be produced by bearing plates.

The following tests will be made to evaluate the sand properties:

(1) Sieve analysis to define the grain size distribution.

(2) Maximum and minimum sand density to determine the parametric limits of soil behavior.

(3) Direct shear tests of sand for dense and loose conditions to determine the angle of internal friction as a function of relative density.

(4) Angle-of-repose of compacted sand to define the limiting slope and stability conditions of the sand surface.

c. Sand bed preparation. The most important controlling factors of soil placement relate to the uniformity and repeatability of soil structure formation to set the test results on an equal basis. To this end, a simple procedure using the soil hopper permits control of the sand density at all levels of soil bed preparation (Fig. 4). The sand is compacted by its own weight falling through the hopper.

The main factors controlling density of sand deposition are the rate (weight deposited per unit time) and height of the flow. For a constant flow height, an increase of the rate of flow will decrease the density of the sand. The rate of flow has a more predominant influence in the soil density outcome than the variation of flow height. For instance, a height of 32 ± 2 in. produces less than 1% variation in density. Dust conditions have been practically eliminated by selecting a sand mixture with less than 1% passing sieve No. 200 by weight and a maximum fall height of 32 in.

After the box is filled to the prescribed level, its surface is smoothed out. Control weights are taken using a load cell and an SR-4 gage.

d. Bearing plates and loading ram. The bearing plates are made of aluminum. A variety of shapes and sizes can be used limited by the boundary influences of the testing box walls. Rectangular plate aspect ratio is 1/5 to simulate a uniformly loaded long strip in plane deformation.

A common fixture supports all bearing plates and a carriage permits unrestricted horizontal displacement to occur simultaneously with the vertical displacement. The horizontal carriage may be locked to produce only vertical displacements (Fig. 5).

5. Pressure–Sinkage Test

The sand test box is set on the loading machine verifying that the bearing plate and soil surface are parallel. The compressive vertical load is applied at a penetration rate of 0.5 in./min and unloaded at 0.05 in./min. Loads, pressures, and displacements are automatically and continuously recorded by two x–y plotters that record load versus horizontal and vertical displacement.

6. Testing Plan

Four groups of bearing plate tests are planned. These are identified by their configuration as rectangular, square, circular, and wheel tests. At least two load penetration tests are required on different sizes of the same plate configuration in order to determine significant pressure–sinkage relations. The minimum number of tests

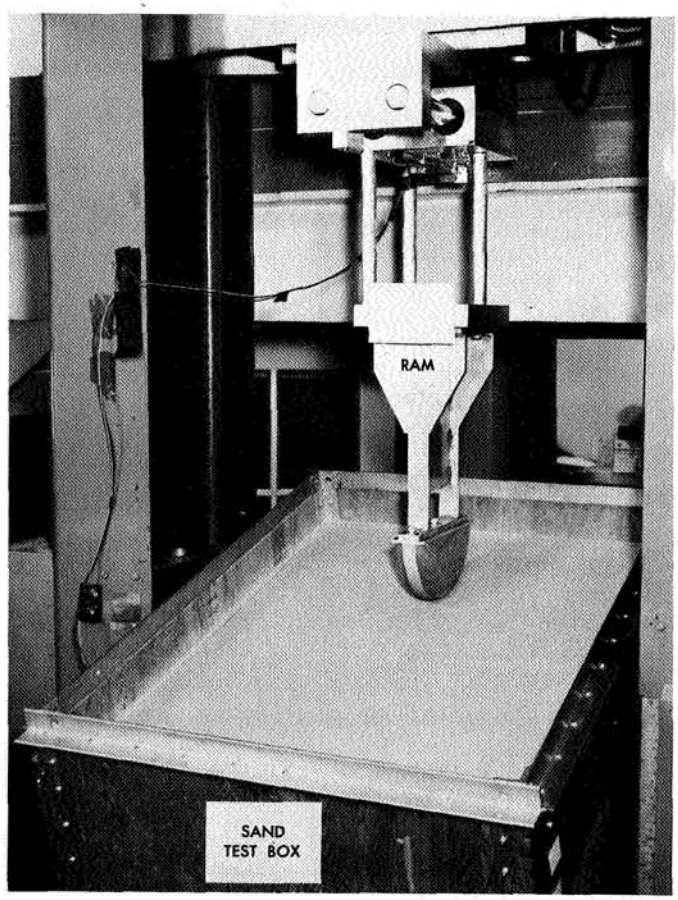

Fig. 5. Fifteen-degree-slope surface test (wheel up–down slope) with wheel raised

required results from the combination of plate shape, size, slope angle and initial plate level below the soil surface (Table 1).

7. Initial Exploratory Tests

Some initial soil tests were made to check out the experimental equipment. These clearly demonstrate the effect of soil slope on the pressure–sinkage relationship and bearing capacity of loaded wheels and flat plates on frictional-type soils. The test soil used was coarse medium-to-fine silica sand with a density of 105 lb/ft^3.

Segments of a wheel, 10 in. diam × 2.5 in. wide, were attached to the loading ram (Fig. 5). Load penetration tests were made for loads applied vertically at a constant penetration rate of 0.5 in./min on both horizontal as well as 15-deg sloped soil surfaces. Vertical, as well as horizontal, displacements were recorded using a special ball-bearing supported loading carriage that permitted free horizontal displacement of the loading fixture. Thus, the wheel segment follows the soil surface failure pattern simulating a free-loaded, non-rotating wheel on a slope.

Results of these early tests for the wheels oriented across the 15-deg slope side, as well as up the slope face, are shown in Fig. 6. With this limited information, it is clear the slope effect on soil properties is considerable even at this low slope angle (15 deg) relative to the angle-of-repose (30 deg). Preliminary tests were also made with rectangular plates (2.0 × 10.0 in., Fig. 7). The results point out the same controlling slope influence on

Table 1. Test plan for plate configuration

Plate shape	Size, in.	Slope, deg	Depth below soil surface, in.	Number of tests
Rectangular	2.00 × 10.00 3.00 × 15.00	0 15 30	0 1 1.5	18
Square	3.54 5.00	0	0 1 1.5	6
Circular (diam)	4.00 5.64	0 15 30	0 1 1.41	18
Rigid wheels (wood) (diam × width)	10 × 2.5 14 × 3.5	0 15 30	— — —	18

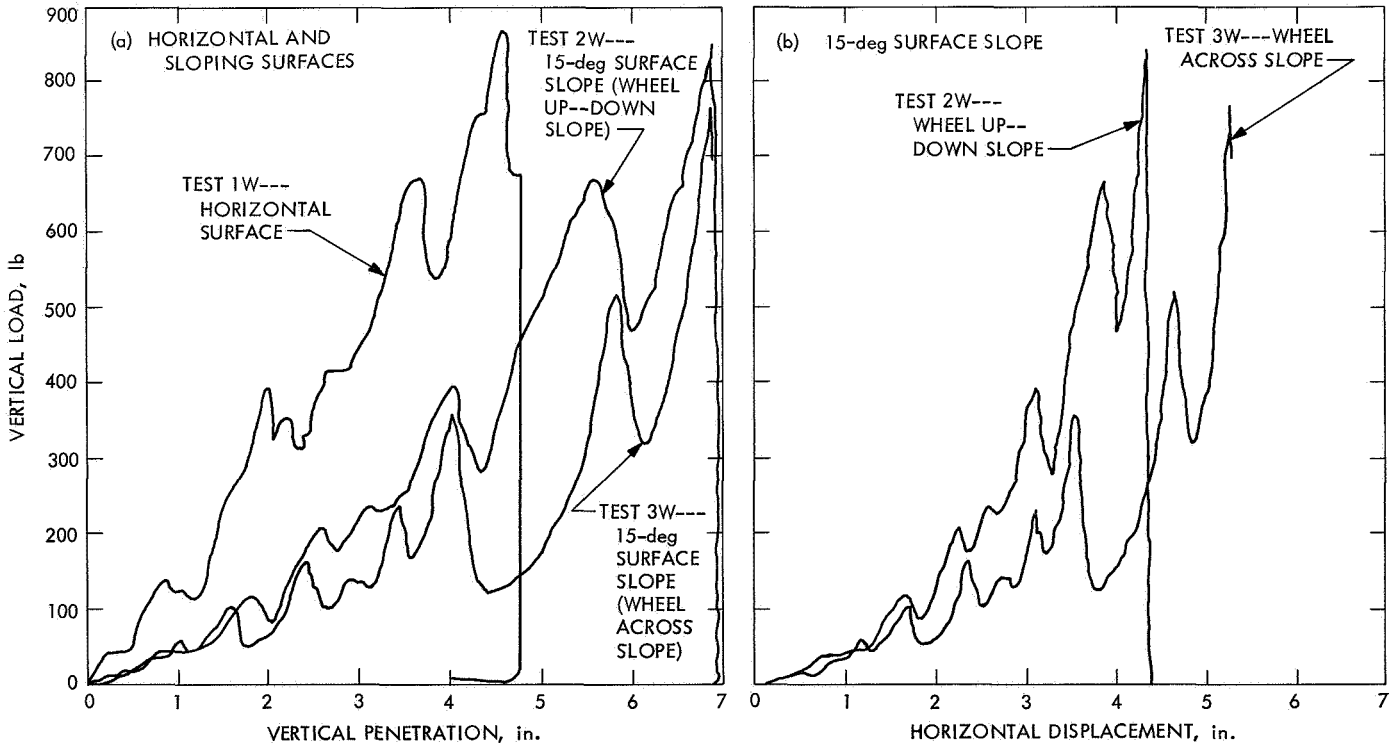

Fig. 6. Wheel–load sinkage test results (10.0-in.-diam × 2.5-in.-width wheel)

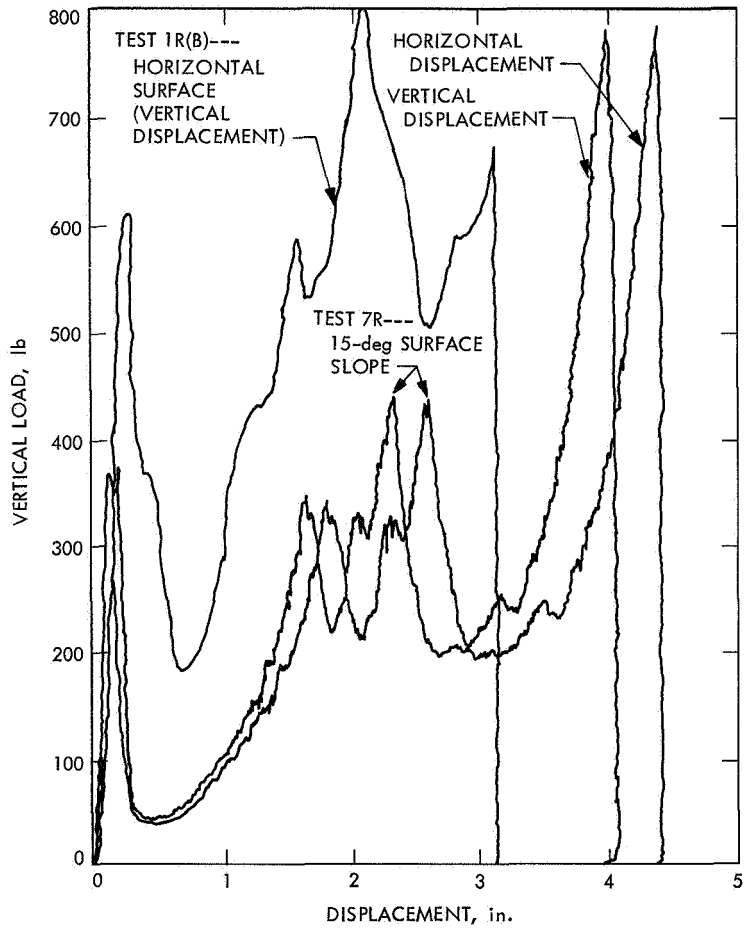

Fig. 7. Preliminary tests made with rectangular (2- X 10-in.) plates

bearing capacity and displacements. The principal conclusions of these exploratory tests are as follows:

(1) Significant degradation of bearing capacity due to slope influence occurs even at relatively low surface slopes compared to the soil angle-of-repose.

(2) Reduction of load support capabilities due to slope effect is accompanied by increased displacements. Horizontal and vertical displacements are of comparable magnitudes and importance in sloped surface tests, whereas the vertical displacements predominate on horizontal surfaces. The total vector displacement of a sloping surface does not coincide with the load direction.

(3) Current mobility concepts refer only to horizontal terrains and these concepts will have to be re-evaluated and extended to include slope effects. In particular, new concepts of soil thrust, mobility resistance, and slip on sloping terrains must be investigated to properly model and evaluate planetary roving vehicle mobility performance.

(4) Vehicle operational safety on slopes is largely impaired due to excessive sinkage. Since vehicle design performance is highly dependent on slopes, further analysis and tests must be done to disclose preferred relative wheel–slope orientation to obtain optimum performance.

References

1. Sokolovsky, V. V., *Statics of Soil Media,* London, Butterworth, 1956.
2. Terzaghi, K., *Theoretical Soil Mechanics,* John Wiley & Sons, 1943.
3. Mayerhof, G. G., "The Ultimate Bearing of Foundations," *Geotech.*, Vol. 2, p. 301, 1951.
4. Mayerhof, G. G., "The Bearing Capacity of Footings Under Eccentric and Inclined Loads," in *Proceedings of the Third International Conference on Soil Mechanics and Foundation Engineering,* Vol. 1, p. 440, 1953.
5. Mayerhof, G. G., "The Ultimate Bearing Capacity of Foundations on Slopes," in *Proceedings of the Fourth International Conference on Soil Mechanics and Foundation Engineering,* Vol. 1, p. 384, 1957.
6. Karafiath, L. L., and Nowatzky, E. A., *A Study of the Effect of Sloping Ground on Bearing Strength and the Landing Performance of Space Vehicles,* Grumman Research Department Memorandum RM 407. Mar. 1968.
7. Shield, R. T., "On Coulomb's Law of Failure in Soils," *J. Mech. Phys. Solids,* Vol. 4, pp. 10–16, 1955.